ROTOR STATE EVALUATION AND STRUCTURAL HEALTH MONITORING THROUGH STRAIN SENSORS

Giovanni Bernardini, Roberto Porcelli, Jacopo Serafini
Roma Tre University, Department of Engineering
Roma, Italy

Pierangelo Masarati
Politecnico di Milano, Department of Aerospace Science and Technology
Milano, Italy

Abstract

This paper presents an original combined approach to shape-sensing and structural health monitoring of helicopter rotors. It is based on the measurement of strain in a limited number of points over the blade surface. The Shape-Sensing algorithm is modal-based and capable of reconstructing nonlinear, moderate lag, flap and torsion deflections. Two Structural Health Monitoring algorithms are presented, one in the time domain and the other in the frequency domain. Both are based on the analysis of the discrepancies between the strains arising in the damaged and the undamaged blades. Two damage types have been considered: a mass unbalance and a localized stiffness reduction. Both Shape Sensing and Structural Health Monitoring capabilities have been tested by numerical simulation using a multibody dynamic solver for general nonlinear comprehensive aeroelastic analysis.

1 INTRODUCTION

Rotor blades are subject to significant deformations in standard and critical operating conditions, owing to aerodynamic and inertia loads. They are slender structures, whose flapping deformation is used to direct rotor thrust and to reduce aerodynamic asymmetry between the advancing and retreating sides of the rotor and thus reduce vibratory loads transmitted to the airframe. Blade shape sensing and structural health monitoring[1] are thus desired features of future helicopters to reduce the need of costly (both in terms of time and money) periodic inspections[2] and to improve flight control system performance[3;4;5]. An increase in flight safety is also expected, since it has been estimated that about 3% of helicopter accidents are caused by failure in the rotor system[6].

Although the potential benefits of placing sensors on rotor blades are very clear, two big issues remain open: (i) the optimal positioning of the sensors on the blade, associated with the risk of accidental breaks during manufacturing or operational life, as well as with the the need to avoid bonding delamination (see[7] for a complete review of technological issues for the case of sensor application on wind turbines); (ii) the most efficient way of powering and connecting sensors, in relation with the rotational motion of the rotor. Both these issues make the use of a large number of sensors significantly more complex than in fixed wing applications. Mainly owing to these reasons, most non-destructive damage detection techniques currently in use are carried out in dedicated facilities and rely upon visual or localized experimental methods, such as acoustic or ultrasonic methods, radiography, X-ray or thermal field methods, which require the knowledge of the damage location as well as its accessibility[8]. In the last years, to overcome limitations imposed by these methods, research has focused on the development of damage identification procedures based upon the detection of changes in the structure vibratory behavior (namely natural frequencies, mode shapes and modal damping).

Following the approach introduced in Refs.[9;10], in this work the authors propose the use of a limited number of strain gauge measurement points for the real-time determination of blade shape and/or health monitoring and blade balancing, following the criteria of multi-purpose sensors. Due to both the low cost and reduced weight of the sensors needed to implement such techniques, their range of applicability can be greatly increased, extending their application also to lightweight helicopters, whose overall safety level could be significantly improved.

2 SHAPE SENSING ALGORITHM

Shape sensing from strain measurement is an area of growing interest in recent years in many fields of application, ranging from automotive to civil engineering. Indeed, while a direct optical measurement (photogrammetry) represents a viable option in some cases[11], it may suffer from practical disadvantages: (i) only in-sight parts of objects may be monitored; (ii) optical markers field of view must be sufficient, i.e. marker plane must form a sufficiently great angle

with the direction between camera and marker itself; (iii) operating conditions (water, ice, absence of light or direct sun exposure of the camera) make the measurement problematic; (iv) for real-time, high speed measurements, expensive equipment is required; (v) camera vibrations heavily affect the accuracy of the measurement. All these problems are harshly present in rotor blade shape reconstruction, making the application of optical measurements very difficult.

On the other hand, Fiber Bragg Gratings strain gauges represent a great improvement in terms of bandwidth and ease of installation with respect to traditional electric resistance solutions. In particular, they drastically reduce the need of cables, as a single fiber may host hundreds of measurement points, whereas each traditional strain gauge needs a dedicated wiring.

Several numerical approaches have been recently proposed for the determination of the deformed shape of bodies from strain measurement; some of them are based on the direct integration of data[12;13], whereas others use modal expansion, exploiting the use of preliminary FEM analysis on the monitored object[14;15;16]. The latter are usually more efficient in terms of number of required sensors, but need the knowledge of the object structure. Moreover, with notable exceptions[17], the approaches in the literature are inherently linear, whereas the general relation between strain and displacement is nonlinear. The modal shape functions may be conveniently evaluated for helicopter rotor blades through an equivalent 1D beam model. However, for linear approaches, rotors may be a challenging application, being subject in standard operating conditions to moderate deflections. Analogous considerations may be drawn for fixed wing aircraft which are becoming more and more flexible.

In the present work, the authors propose a modal shape sensing approach, capable of reconstructing the complete deformation of a beam-like structure, including torsion, in-plane, and out-of-plane bending. It is capable of handling nonlinear terms up to second order. This is particularly interesting for flight dynamics and aeroelastic control applications, in which the knowledge of limited information on rotor kinematics may give unsatisfactory results. It is worth mentioning that, at present, devices of the latter type (e.g. measuring cyclic flapping components β_c and β_s), or flapping-related displacement on a point along the blade) are still under development[11].

2.1 Strain-displacement relationship

Let us consider the approximation proposed in[18] for the strain-displacement relationship of a twisted beam, which is valid for moderate deflections

$$\begin{aligned}\varepsilon_{\xi\xi} = {} & u' + \frac{1}{2}(v'^2 + w'^2) + (\eta^2 + \zeta^2)\left(\theta'\phi' + \frac{\phi'^2}{2}\right) \\ & - v''[\eta\cos(\theta+\phi) - \zeta\sin(\theta+\phi)] \\ & - w''[\eta\sin(\theta+\phi) + \zeta\cos(\theta+\phi)]\end{aligned} \tag{1a}$$

$$\varepsilon_{\xi\eta} = -\frac{\zeta\phi'}{2} \tag{1b}$$

$$\varepsilon_{\xi\zeta} = \frac{\eta\phi'}{2} \tag{1c}$$

where η and ζ are the cross section principal axes, ξ is the coordinate along the elastic axis, u, v, w are the axial, lead-lag and flap displacements of the elastic axis, whereas θ and ϕ are the built-in twist angle and the blade cross-section elastic rotation (torsion), respectively. Note that in the above equations the warping function has been neglected, since its effect is deemed negligible in rotor blade dynamics.

In the proposed formulation, the displacement $\boldsymbol{\delta} = \{u, v, w\}^T$ and the elastic torsion angle ϕ are first expressed as the linear combination of suited shape functions

$$\boldsymbol{\delta}(\xi, t) = \sum_i q_i(t)\boldsymbol{\Psi}_i(\xi) \tag{2a}$$

$$\phi(\xi, t) = \sum_i r_i(t)\Phi_i(\xi) \tag{2b}$$

Then, using M shape functions to approximate the torsion angle, Eqs. (1b) and (1c) are rewritten as

$$\varepsilon_{\xi\eta} + \varepsilon_{\xi\zeta} = \boldsymbol{K}\boldsymbol{r} \tag{3}$$

where $\boldsymbol{r} = \{r_1, r_2, \ldots, r_M\}^T$ contains the torsion amplitudes and $\boldsymbol{K}$ is a row vector evaluated in a straightforward manner from the knowledge of the torsion shape functions and the location of the evaluation point. Once the torsion amplitudes are obtained exploiting Eq. (3), Eq. (2b) is used to calculate the terms depending on ϕ in Eq. (1a), leaving the displacement components as the only unknowns.

Finally, using N shape functions to approximate $\boldsymbol{\delta}$, evaluating Eq. (1a) at two points of the same cross section, and subtracting the corresponding $\varepsilon_{\xi\xi}$ values, a purely linear relationship between the difference $\Delta\varepsilon_{\xi\xi}$ and $\boldsymbol{q} = \{q_1, q_2, \ldots, q_N\}^T$ is obtained

$$\Delta\varepsilon_{\xi\xi} = \boldsymbol{H}\boldsymbol{q} + b \tag{4}$$

where $\boldsymbol{H}$ is a row vector depending on the displacement shape functions, $\boldsymbol{\Psi}_i$, the torsion angle and the location of the evaluation point, whereas b is a constant term depending only on the torsion angle and the location of the evaluation point.

It is worth noticing that, using $\Delta\varepsilon_{\xi\xi}$ instead of $\varepsilon_{\xi\xi}$ for the evaluation of the elastic axis displacement, the contribution of the axial displacement u vanishes, thus reducing the number of total modes required for blade shape reconstruction.

2.2 Torsion and displacement amplitude identification

In order to identify torsion and displacement amplitude from Eqs. (3) and (4), $N+M$ linearly independent equations are needed. These equations can be obtained by performing N measurements for ε_{12} and/or ε_{13}, and M measurements for $\Delta\varepsilon_{\xi\xi}$ at different cross-sections along the blade span. However, owing to the presence of noise and measurement errors in both the signal acquisition/processing and sensor positioning processes, a larger number of measurements should be used to obtain a reliable evaluation of the modal amplitudes. For both the torsion and bending problems, this yields overdetermined problems, whose solutions may be obtained in a least-squares sense as

$$\boldsymbol{r} = K^{+}(\boldsymbol{\epsilon}_{\xi\eta} + \boldsymbol{\epsilon}_{\xi\zeta}) \tag{5}$$

and

$$\boldsymbol{q} = H^{+}(\Delta\boldsymbol{\epsilon}_{\xi\xi} - \boldsymbol{b}) \tag{6}$$

where $(\cdot)^{+}$ indicates the Moore-Penrose pseudo-inverse.

Notice that the evaluation of $\Delta\varepsilon_{\xi\xi}$ requires at least two strain gauges for each cross section, with a definite increase in the number of sensors (one per section) with respect to those used in classical modal approaches (see for example[15]), which are equal to the number of modes. This drawback is largely compensated by the fact that the proposed procedure is computationally very efficient, as it solves a nonlinear elasticity problem (under the assumption that bodies are subject to moderate deformations) through the sequential solution of two linear algebraic systems (Eqs. (5) and (6)). Furthermore, it appears to be quite accurate since, due to error propagation, a single $\Delta\varepsilon_{\xi\xi}$ measurement is statistically more precise than an $\varepsilon_{\xi\xi}$ one.

Finally, some details are needed about the simulation of a real strain gauge measurement. Considering a set of sensors glued over the blade surface, and oriented at angles α_i with respect to the ξ-axis, their outputs $\varepsilon_{\alpha_i\alpha_i}$ over each cross section are used to evaluate $\varepsilon_{\xi\xi}$, $\varepsilon_{\xi\zeta}$ and $\varepsilon_{\xi\eta}$ in that section. Indeed, from the strain tensor associated with the Euler-Bernoulli beam

$$\boldsymbol{T} = \begin{bmatrix} \varepsilon_{\xi\xi} & \varepsilon_{\xi\eta} & \varepsilon_{\xi\zeta} \\ \varepsilon_{\xi\eta} & -\nu\varepsilon_{\xi\xi} & 0 \\ \varepsilon_{\xi\zeta} & 0 & -\nu\varepsilon_{\xi\xi} \end{bmatrix}$$

the local strain along a direction tangent to the beam surface, identified by the unit vector $\boldsymbol{m}$ (see Fig. 1), is given by

$$\begin{aligned} \varepsilon_{mm} = (\boldsymbol{T}\boldsymbol{m})\cdot\boldsymbol{m} = \varepsilon_{\xi\xi}[(1+\nu)m_\xi^2 - \nu] \\ +2\varepsilon_{\xi\eta}m_\xi m_\eta + 2\varepsilon_{\xi\zeta}m_\xi m_\zeta \end{aligned} \tag{7}$$

where $\{m_\xi, m_\eta, m_\zeta\}$ are the components of $\boldsymbol{m}$.

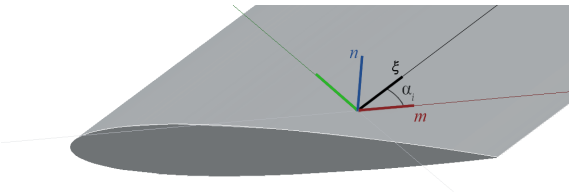

Figure 1: Sensor orientation.

Notice that, being the twist of a helicopter blade relatively small, the optimal sensor orientation to obtain $\varepsilon_{\xi\eta} + \varepsilon_{\xi\zeta}$ in Eq. (5) from the difference of the signals of two sensors located at the same measurement point, is $\alpha_i \approx \pm 45^\circ$. Notice also that the sum of the signals of the above sensors may be used to evaluate $\varepsilon_{\xi\xi}$. Considering all the $N+M$ modes, the minimal set of sensors required for the solution of Eqs. (5) and (6) is of M pairs of $\pm 45^\circ$ sensors and (at least) $N-M+S$ sensors aligned with the blade span ($N-M$ sensors to reach the number of N $\varepsilon_{\xi\xi}$ sensors, plus one additional sensor per section, for a total of S sensors, which are needed to measure an additional $\varepsilon_{\xi\xi}$ value for each section, to be used in the evaluation of $\Delta\varepsilon_{\xi\xi}$).

Although a redundant set of sensors is required anyway, to reduce the influence of measurement errors, for typical rotorcraft applications a limited number of sensors should be required, since only few modes (in the order of ten) are sufficient to accurately reconstruct the shape of the rotor blades.

3 STRUCTURAL HEALTH MONITORING ALGORITHMS

Structural Health Monitoring (SHM) has been extensively studied in the last two decades in almost every field of engineering. In Refs. 19;20;21;22;23, a broad selection of methodologies are presented, whereas Ref. 2 presents a review of SHM methodologies for rotorcraft. Despite the differences, in terms of measured quantities and data post-processing techniques used to predict and locate a damage, two fundamental concepts are always present: (i) a reference state is necessary to compare the degraded performance with; (ii) high frequency phenomena can pinpoint more accurately the location of the damage. In both cases, helicopter rotors in steady-state flight conditions are a favorable field of application, due to the presence of multiple blades (ideally identical) experiencing the same low- to high-frequency excitation with a very small phase shift between them.

In this paper, two different criteria for blade damage detection based on the comparison of signals from sensors located on different blades are proposed. The properties investigated by the authors are: (i) sensitivity to structural modifications; (ii) proneness to false positives and negatives due to unsteady flight conditions. The first criterion proposed is based on the evaluation of Welch's power spectral density[24] of signals obtained as the difference between

strain measurements from sensors in the same position on different blades. Indeed, in the absence of a blade damage/imbalance with respect to the other ones, it is expected that the blade steady-state aeroelastic responses do not differ, once the signals from the blades are phased by their relative angles ($2\pi(i-j)/N_b$, for i-th and j-th blades).

Moreover, the power spectral density of each blade response is characterized by contributions at frequencies $i\Omega$ (where Ω is the rotor angular velocity and $i \in \mathbb{N}_0$), due to steady response, and $\omega \pm i\Omega$ (where ω is a generic blade eigenfrequency), due to transient response. Since in helicopter applications the rotor eigenfrequencies are separated by design from multiples of the rotor angular velocity, in order to avoid resonance, monitoring $i\Omega$ peaks in the blade response is expected to be a suitable criterion for damage identification. In fact, the amplitudes of the PSD peaks of the signals obtained as the difference between strain measurements from different blades (Δ-signal), at frequencies $i\Omega$, are expected to be persistent in time in damaged systems, as opposed to the peaks associated with the transient response of an undamaged system (strongly dependent on lightly damped lag modes), which are expected to show a pronounced time dependence.

The second proposed criterion is based on the autocorrelation of the Δ-signals, namely

$$c_{ij}(\tau) = \frac{1}{T}\int_{-T/2}^{T/2} \Delta s_{ij}(t)\Delta s_{ij}(t+\tau)d\tau \tag{8}$$

Since the difference between two undamaged blades (assumed identical) contains only noise and transient effects, it is expected that, considering a sufficiently long sampling period, the normalized autocorrelation is very low, except when zero time shift is considered. On the contrary, for a Δ-signal involving a damaged blade, the autocorrelation should be high (or low) also for other values of the time shift, as it may be easily verified for two periodic analytical signals. Notice that in real-life cases there are dissimilarities between rotor blades as a result of the manufacturing process or of environmental effects, which are mitigated and maintained below acceptable tolerances by tracking. Hence, in this case a non-zero Δ-signal is present also in undamaged systems. To overcome this problem, both criteria are applied to the signal

$$\Delta\Delta s_{ij}(t) = \Delta s_{ij}(t) - \Delta s_{ij}^{\text{ref}}(t) \tag{9}$$

namely the variation of the Δ-signal with respect to the reference state ($\Delta\Delta$-signal).

4 NUMERICAL RESULTS

The test cases considered in this section are hingeless rotor blades inspired to that of the Bölkow (now Airbus Helicopters) BO105 helicopter, with a main rotor radius of 4.9 m rotating at 44.4 rad/s, and in forward-flight condition at an advance ratio (the ratio between the forward velocity and the blade tip velocity in hover) $\mu = 0.2$. The first blade analyzed is uniform, whereas the second one is realistically non-uniform, having a maximum variation of the bending stiffness of about $24000\,\%$, considering also the blade root and the flexbeam. Figure 2 illustrates the qualitative trend of the main structural properties along the blade.

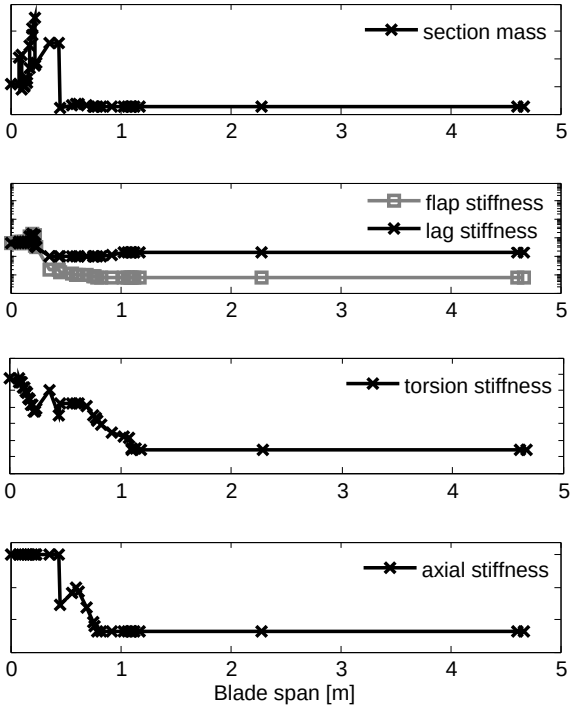

Figure 2: Structural properties along blade.

The actual measurements on the rotor blades are simulated using numerical results computed by means of dynamic and aeroelastic simulations performed with the free, general purpose multibody dynamics solver MBDyn[25]

4.1 Shape Sensing

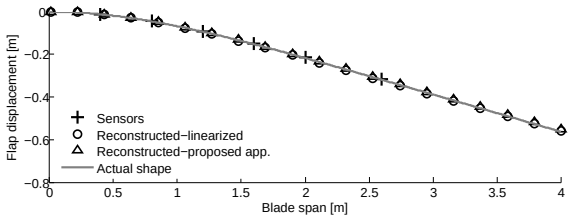

Figure 3: Shape reconstruction for a small-displacement flap bending. Comparison between linearized and proposed approach.

The first analysis performed is the flap-wise bending reconstruction of a non-rotating blade with NACA0012 airfoil. In Fig. 3, the results of the proposed approach are compared with those of the linearized model for small displacements.

Unless otherwise stated, here and in the following, two pairs of $\pm 45^\circ$ sensors over the same section are considered ("measurement section", in the following) for both

blade upper and lower surfaces. Notice that this is not an optimal sensor arrangement, which would require a dedicated analysis. Some authors[26] have proposed the use of the condition number (CN) of matrices H and K as an estimate of the quality of sensor placement. In addition, it should be noticed that optimal positioning should also take into account the expected value of the measurement, to improve the signal to noise ratio.

Two and three bending modes are respectively used for the definition of the H and K matrices of Eqs. (5) and (6). The analytical mode shapes from a homogeneous beam are considered. In this case, the proposed formulation is equivalent to the classic modal approach to shape sensing, as expected, since the nonlinear terms are negligible. Analogous results (not shown here, for conciseness) have been obtained for the lag deformation.

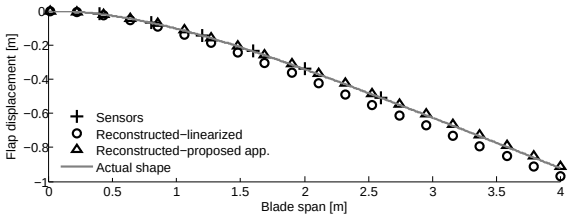

Figure 4: Shape reconstruction for a moderate-displacement flap bending. Comparison between linearized and proposed approach.

On the contrary, when displacements become larger, the effect of the nonlinear terms is no longer negligible. In this case, illustrated in Fig. 4, the proposed approach provides a much more accurate shape reconstruction.

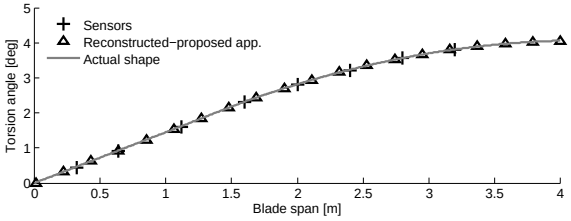

Figure 5: Shape reconstruction for a torsion-forced beam.

Figure 5 shows the reconstruction of the torsion deformation of the same blade. Here only the result from the proposed approach is shown, since the torsion problem stated in Eqs. (1b) and (1c) is linear.

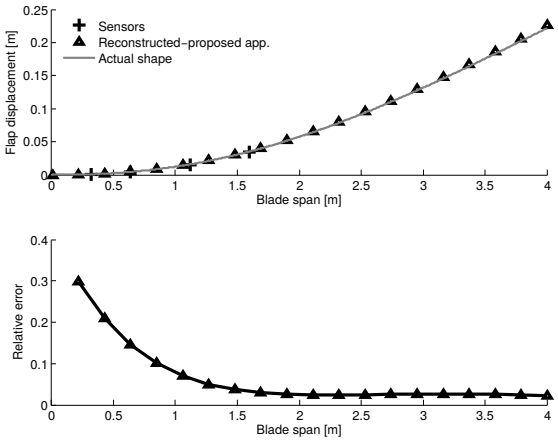

Figure 6: Flap reconstruction using sensors near the blade root.

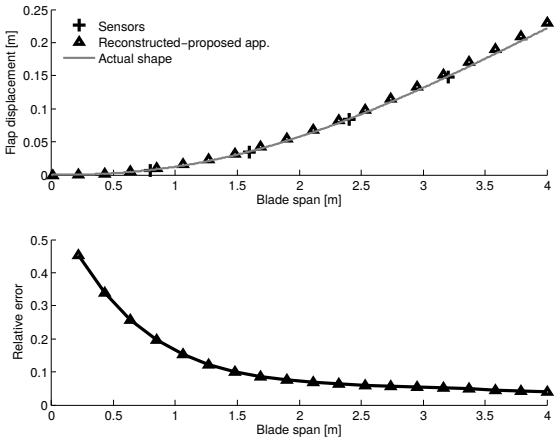

Figure 7: Flap reconstruction using sensors uniformly distributed along the blade.

Figures 6 and 7 depict the effect of the spanwise position of the sensors, both in terms of flapwise bending reconstruction and relative error. In Figure 6, four sensors are clustered near the blade root section, whereas in Figure 7 the same number of sensors are uniformly distributed over the whole span. As expected, placing the sensors closer to the root, where the strains associated with low-frequency modes are usually larger, reduces the reconstruction error.

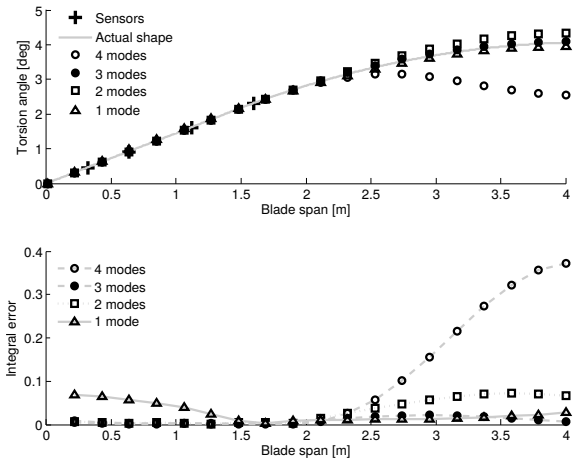

Figure 8: Torsion reconstruction varying number of modes.

Figure 8 presents a sensitivity analysis with respect to the number of modes used in the reconstruction algorithm. It depicts the torsion deformation obtained by increasing the number of the torsion modes, and using the four sensorized sections clustered near the blade root. Expanding the modal base up to three modes gives an improvement of the reconstruction quality, whereas the use of four modes seems to produce a dramatic worsening of the accuracy. The same analysis performed on flap and lead-lag deformations (not presented here for the sake of conciseness) shows that the optimal number of modes is two, although the sensitivity of the reconstruction accuracy to the modes number is less pronounced. The negative effect of increasing the number of modes fixing the number of sensors can be also inferred by Tab. 1, which reports the condition number of the H and K matrices when the modes number is varied. Here the number of sensors per section has been kept to a minimum, which is equal to three, assuming that two sensors are used for evaluating torsion and bending at the same time (subtracting and adding their signals). Globally, the modes increase results in a degradation of the conditioning of the matrices, which become ill-conditioned when four modes are used. It is worth recalling that the reconstruction accuracy is a trade-off between a well-conditioned system and an appropriate number of modes. If a high number of modes is required due to the nature of the problem, a simultaneous increase of the number of sensors is needed, taking care to position them in a suited way to keep the condition number low.

Table 1: Condition number of H and K matrices for different bending and torsion modes number (four sections, three total sensors per section).

	1	2	3	4
H	1	15.82	9.80e02	2.61e05
K	78.74	1.59e03	6.53e02	8.60e06

Thus far, a homogeneous blade has been considered. In other words, the modal base used for the definition of the H and K matrices of Eqs. (5) and (6) is the proper base for the problem examined. If we consider a non-uniform blade in the simulation, the overall quality of the shape reconstruction is expected to decrease, for a fixed number of modes (Figs. 9 and 10).

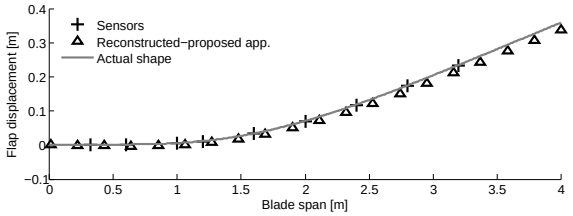

Figure 9: Shape reconstruction of a non-uniform blade, using modes of a uniform one.

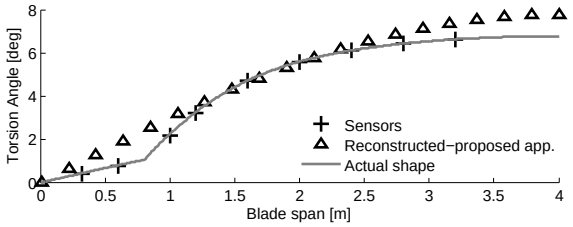

Figure 10: Shape reconstruction of a non-uniform blade, using modes of a uniform one.

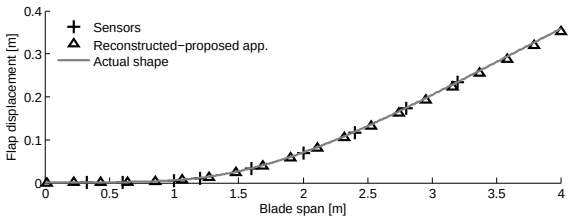

Figure 11: Shape reconstruction of a non-uniform blade, using its natural modes.

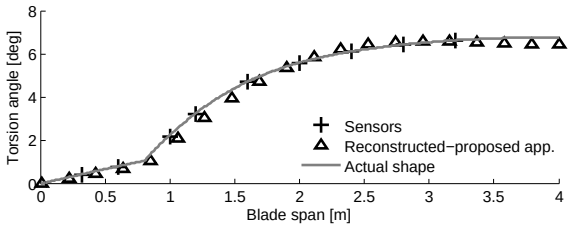

Figure 12: Shape reconstruction of a non-uniform blade, using its natural modes.

However, using accurate blade mode shapes, computed for the actual non-uniform blade, the reconstruction accuracy is essentially restored, as shown in Figs. 11 and 12. Since for real-life applications a FEM model of the blade

is usually available, the evaluation of its eigenmodes is a convenient operation, which reduces the number of modes that need to be considered (and thus of the sensors to be installed). Another issue that is addressed here is the influence of measurement noise on the robustness of the result. In particular, the effect of redundant measurement sections on disturbance rejection has been investigated.

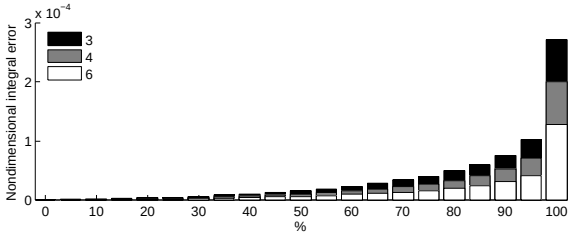

Figure 13: Percentiles of error for different number of sensors over each measurement section.

Considering a random noise equal to 0.2×10^{-6} plus 10% of the measurement (which is a value significantly higher than that expected for a modern strain sensor), the reconstruction error for a flap bending case has been evaluated over ten thousand simulations with different numbers of couples of $\pm 45^{\circ}$ sensors for each measurement section. Figure 13 shows the resulting percentiles of integral error (namely $\frac{1}{L^3}\int_0^L \left(w_r - w_s\right)^2 dx$). From the figure it is clear that by increasing the number of sensors, the error is significantly reduced.

In the following, the focus is on dynamical results. Figure 14 shows the tip-flap displacement for a periodically forced, yet non-rotating case.

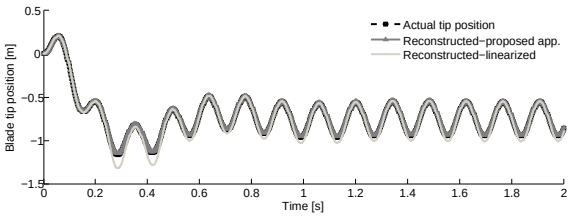

Figure 14: Time history of actual flap displacement of tip and its reconstruction with linearized and proposed approach.

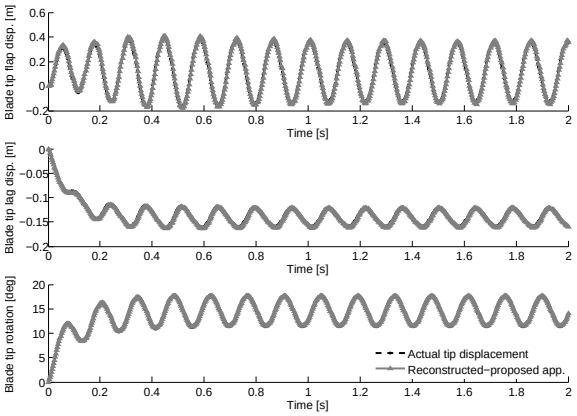

Figure 15: Reconstruction of tip flap, lag and torsion displacements of the rotating blade.

Figure 15 reports the tip displacement components for the rotating blade. In this case, one lag mode, four flap modes and two torsion modes are used in the reconstruction, which uses four measurement sections. As stated in Section "Shape Sensing Algorithm", axial modes are not needed for the proposed approach. On the contrary, with the linearized approach it is strictly necessary to introduce them, since a significant part of strain is due to the centrifugal force field. Figure 16 shows what happens when no axial modes are included in the simulation for the linearized approach. In this case, after introducing a single axial mode, the quality of the reconstruction is restored, as shown in Fig. 17. However, this comes at the cost of an increase of modes that need to be evaluated and thus of the number of required sensors.

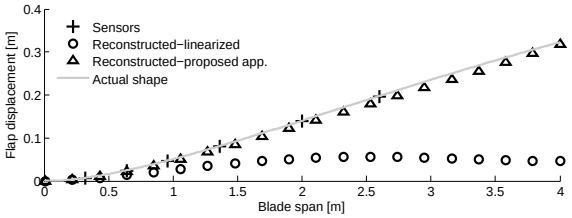

Figure 16: Shape reconstruction of a rotating blade. The linearized approach is here applied without including axial modes.

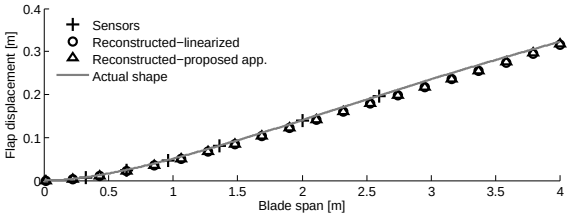

Figure 17: Comparison between proposed approach and linearized one (including axial mode) for a rotating case.

Figure 18 shows the time history of the integral error (defined as above) and the relative error at the blade tip.

Although quite small, the error on flap displacement is significantly larger than those on lag and torsion. Increasing the number of sensorized sections and modes from four to eight (Fig. 19) significantly improves the shape reconstruction. Note that increasing the number of sensors requires a corresponding increase of the sensorized portion of the blade, to maintain a small conditioning number for both the H and K matrices. This caution is needed, since natural modes behave similarly in the vicinity of the blade root.

Notice that a reduction of required modes may also be achieved by considering those of a rotating beam.

It is worth mentioning that the proposed approach could be also applied to subparts (beams) of complex structures. This makes it possible to retain also the evaluation of second order terms in cases where the analytical relationship between displacement and strain is unknown. The drawback is that for the evaluation of the structure's global shape a post-processor is needed, which enforces compatibility of the subparts' deformation.

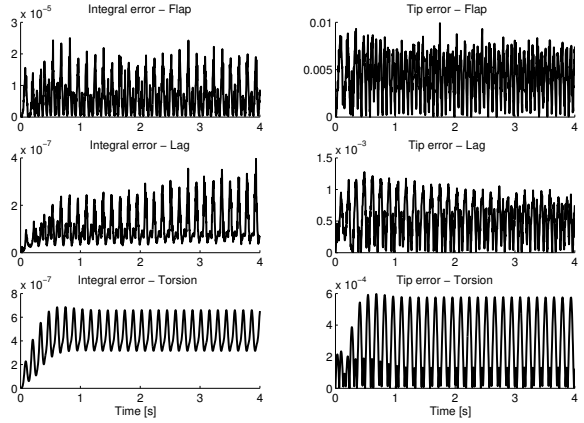

Figure 18: Integral and tip error using one lag, four flap and two torsion modes, considering four sensorized sections.

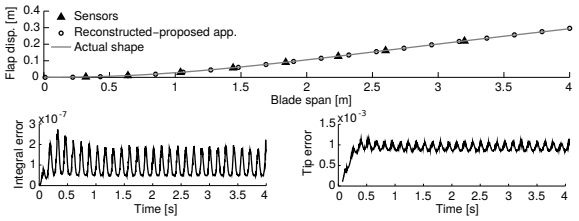

Figure 19: Integral and tip error on flap using eight flap modes, considering eight sensorized sections.

Finally, with the aim of assessing the effectiveness of the shape sensing procedure on complex 3D structures, composed of different structural elements (*e.g.,* 3D elements, beams and shells), the wing box sketched in Fig. 20 has been considered. For this analysis, an approximate distribution of the aerodynamic loads is considered, linearly varying along the wing chord and elliptically varying along the wing span.[27] Nine virtual strain gauges are positioned on the upper skin, in the first third of the wing span from the root (see Fig. 20). Results in terms of spanwise distribution of the out-of-plane displacement are shown in Fig. 21, where results from a FEM analysis are compared with the reconstruction obtained using two modes. Note that in this case the accuracy of the reconstruction algorithm is weakly dependent on the number of modes. Indeed, a similar analysis, performed using only one mode for the out-of-plane displacement reconstruction, provided results with less than 1% error at the wing tip.

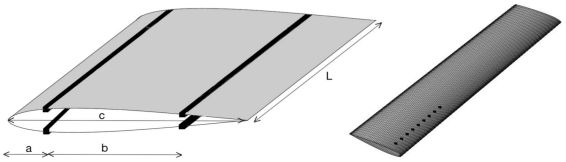

Figure 20: Idealized wing structure (C=1 m, L=6.5 m, a=0.22 m, b=0.57 m). Black dots on the right picture represent measurement points location.

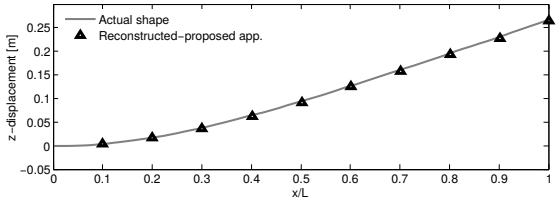

Figure 21: Simulated and reconstructed wing deflection.

4.2 Structural Health Monitoring

Two types of alteration on the blade have been considered with the techniques proposed in section "Structural Health Monitoring Algorithms": (i) variation in mass distribution; (ii) variation in flapping stiffness; The former are representative of an incorrect track and balance procedure, while the latter of a structural damage of the blade.

The mass alteration is simulated by introducing lumped masses at the tip of the blade, whereas the structural damage is simulated by dividing the blade into two beams connected by a rotational joint with a spring that reproduces the residual stiffness in the damaged location. Considering the case of blade flapwise bending (analogous consideration may be made for the torsion), the equivalence between the spring constant and the variation of the stiffness ΔS in a region of length $L_d \ll R$ is stated by the formula:

$$K = \frac{1}{L_d\left[(S-\Delta S)^{-1} - S^{-1}\right]}$$

where S is the undamaged blade stiffness.

4.2.1 Time-domain analysis

The first results show the autocorrelation of the $\Delta\Delta$-signal over 100 revolutions. Note that, although the undamaged

blades are identical, the numerical solution of the aeroelastic simulation introduces systematic discrepancies in the blade response. Thus, even here the use of the $\Delta\Delta$-signal instead of the Δ-signal is beneficial. Figures 22 and 23 clearly show the effect of the addition of 2 and 4 grams, respectively, at the tip of one blade.

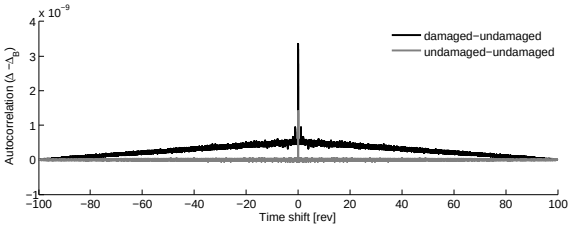

Figure 22: Autocorrelation of $\Delta\Delta$-signal from altered (+2 g @tip) and nominal blades.

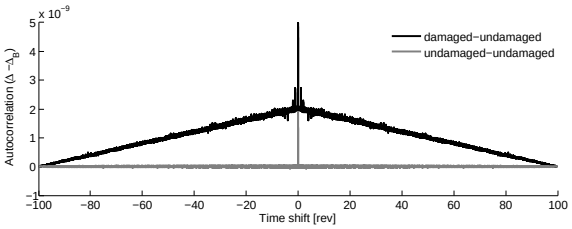

Figure 23: Autocorrelation of $\Delta\Delta$-signal from altered (+4 g @tip) and nominal blades.

Figure 24 shows what happens if the autocorrelation is performed over the Δ-signal instead of $\Delta\Delta$-signal. In this case the damaged blade is no longer recognizable for that value of alteration (2 grams). While the systematic discrepancy between undamaged blades is a purely numerical problem, it is expected that an analogous situation will be present in real-life cases, making the use of $\Delta\Delta$-signal an interesting way to obtain more robust results.

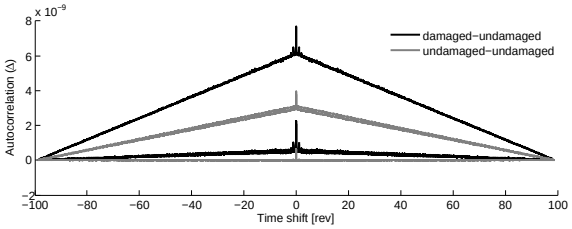

Figure 24: Autocorrelation of Δ-signal from altered (+2 g @tip) and nominal blades.

Complementary information may be drawn from the analysis of mean values of $\Delta\Delta$-signal, shown in Figs. 25 and 26. The presence of blade damage appears clearly in the bars involving blade 1 (the one which is damaged), with almost identical effect. On the contrary, the mean value of $\Delta\Delta$-signal between undamaged blades are more than two orders of magnitude smaller. Figure 27 shows an example of analysis of mean values considering Δ-signal instead of $\Delta\Delta$-signal. As noted before, also in this case the damaged blade is not clearly recognizable.

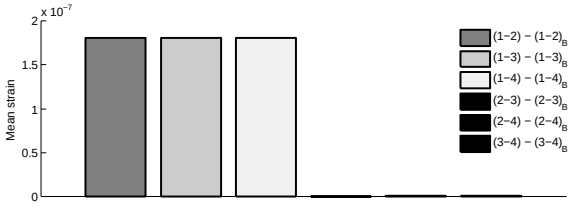

Figure 25: Mean value of $\Delta\Delta$-signal from altered (+2 g @tip) and nominal blades.

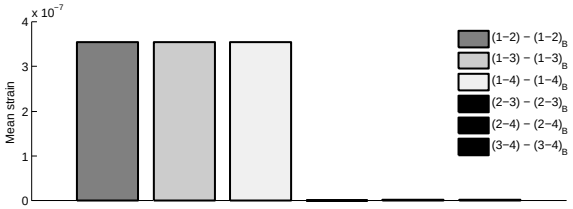

Figure 26: Mean value of $\Delta\Delta$-signal from altered (+4 g @tip) and nominal blades.

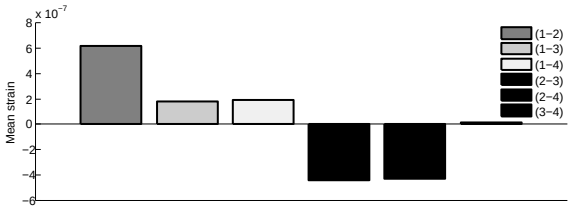

Figure 27: Mean value of Δ-signal from altered (+2 g @tip) and nominal blades.

Figures 28 to 31 show autocorrelation and mean values of $\Delta\Delta$-signal in presence of damage which causes 5% or 10% flapping stiffness reduction on a $1cm$ trait positioned at one third of the blade, leading to analogous considerations.

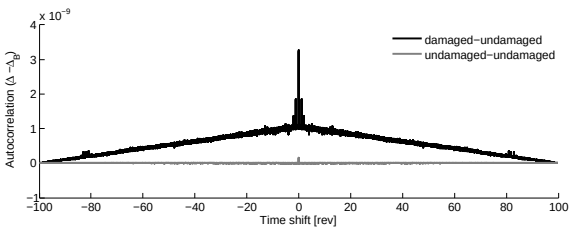

Figure 28: Autocorrelation of $\Delta\Delta$-signal from altered (5% flapping stiffness reduction on 1 cm @$r = 1.53$ m) and nominal blades.

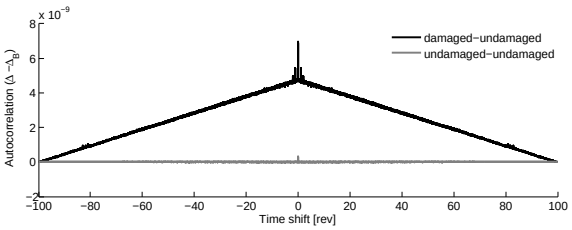

Figure 29: Autocorrelation of $\Delta\Delta$-signal from altered (10% flapping stiffness reduction on 1 cm @$r = 1.53$ m) and nominal blades.

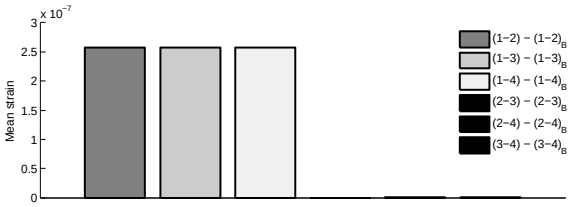

Figure 30: Mean value of $\Delta\Delta$-signal from altered (5% flapping stiffness reduction on 1 cm @$r = 1.53$ m) and nominal blades.

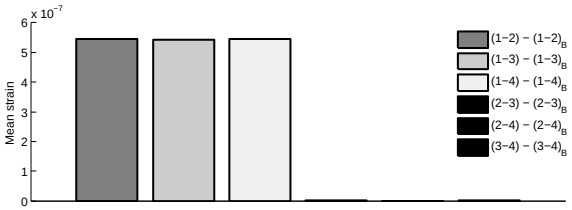

Figure 31: Mean value of $\Delta\Delta$-signal from altered (10% flapping stiffness reduction on 1 cm @$r = 1.53$ m) and nominal blades.

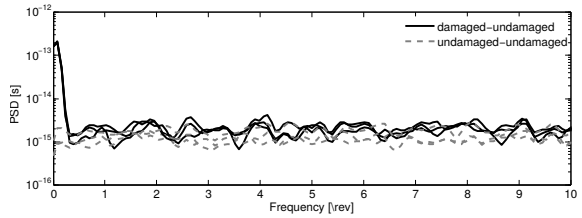

Figure 32: PSD of $\Delta\Delta$-signal from altered (+2 g @tip) and nominal blades.

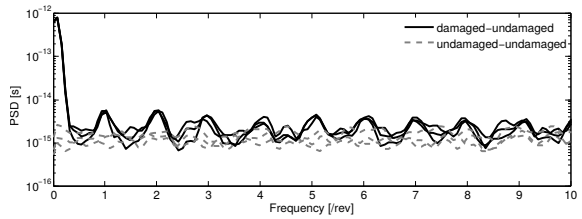

Figure 33: PSD of $\Delta\Delta$-signal from altered (+4 g @tip) and nominal blades.

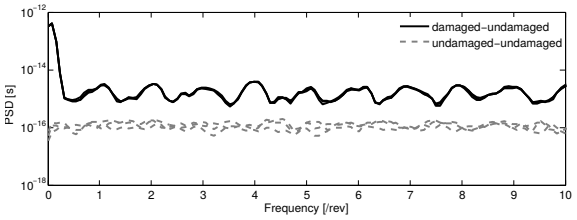

Figure 34: PSD of $\Delta\Delta$-signal from altered (5% flapping stiffness reduction on 1 cm @$r = 1.53$ m) and nominal blades.

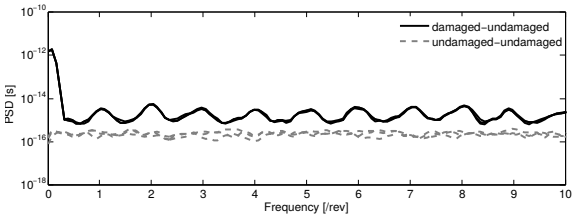

Figure 35: PSD of $\Delta\Delta$-signal from altered (10% flapping stiffness reduction on 1 cm @$r = 1.53$ m) and nominal blades.

4.2.2 Frequency-domain analysis

The same damaged configurations have been investigated also though the frequency domain approach presented in Section "Structural Health Monitoring Algorithms". Figures 32 and 33 show the PSD of $\Delta\Delta$-signal in presence of 2 grams and 4 grams mass at one blade tip, respectively. The PSDs have been obtained through the Welch's algorithm using a 100-revolutions long signal, divided in 10 Blackman-Harris windowed chunks with 50% overlap.

As expected, a great discrepancy between the PSDs of $\Delta\Delta$-signals involving the damaged blade and those not involving it is present at zero frequency. Moreover, from the PSD, it is also possible to highlight other discrepancies of the force (periodic) response at frequency $\Omega, 2\Omega, \ldots, N\Omega$ which are unaffected by transient response if no resonances are present. Peaks at $i\Omega$ are clearly visible in Fig. 33, whereas in Fig. 32 the type and entity of the damage hide this behavior.

When considering the flapping stiffness reduction (see Figs. 34 and 35), the $i\Omega$ peaks are present also for low damage entity, along with the peak for zero frequency. This is probably due to the fact that this kind of alteration affects modes having frequency higher than those affected by the addition of a tip mass.

5 CONCLUSIONS & FUTURE WORK

The numerical testing of the shape-sensing procedure has given good results in terms of accuracy and precision, with a small number of required strain sensors. It has also demonstrated its capability to reconstruct the shape of moderately deflected beams (whereas classical modal

approaches to shape-sensing are limited to small displacements), although the algorithm only requires the solution of linear problems. The determination of the optimal placement of sensors, the capability of dealing with finite displacements and the extension of the algorithm to other basic structural elements (*e.g.* plates, shells) are still open issues that will be the subject of future analyses.
Another field of future study is the application of the proposed procedure to complex structures. In this case, it will be necessary to make information from the shape-sensing consistent across subparts of the structure. The structural health monitoring problem has been addressed using both frequency and time domain analyses applied on the difference of strain signals (Δ-signals) among the blades. The techniques may be applied to the measurements used for the shape sensing algorithm, a positive fact in the scope of an integrated instrumentation lodged on rotor head. The different techniques have shown a good capability to detect blades mass or stiffness alterations, even of small entity. The use of a reference Δ-signal (due to differences among blades caused by fabrication process) is promising in order to reduce false positives. The accuracy and robustness during maneuvered flight in presence of external disturbance will be addressed in the future.

References

[1] C. R. Farrar and K. Worden, "An introduction to structural health monitoring," *Philosophical Transactions of the Royal Society of London A: Mathematical, Physical and Engineering Sciences*, vol. 365, no. 1851, pp. 303–315, 2007.

[2] P. Pawar and R. Ganguli, "Helicopter rotor health monitoring-a review," *proceedings of the institution of mechanical engineers, part G: Journal of Aerospace Engineering*, vol. 221, no. 5, pp. 631–647, 2007.

[3] M. D. Takahashi, "Rotor-state feedback in the design of flight control laws for a hovering helicopter," *Journal of the American Helicopter Society*, vol. 39, no. 1, pp. 50–62, 1994.

[4] J. F. Horn, W. Guo, and G. T. Ozdemir, "Use of rotor state feedback to improve closed-loop stability and handling qualities," *Journal of the American Helicopter Society*, vol. 57, no. 2, pp. 1–10, 2012.

[5] S. Panza and M. Lovera, "Rotor state feedback in the design of rotorcraft attitude control laws," in *Advances in Aerospace Guidance, Navigation and Control*, pp. 205–225, Springer, 2015.

[6] L. Iseler and J. De Maio, "An analysis of us civil rotorcraft accidents by cost and injury (1990-1996)," Tech. Rep. TM-2002-209615, NASA, 2002.

[7] S.-W. Kim, W.-R. Kang, M.-S. Jeong, I. Lee, and I.-B. Kwon, "Deflection estimation of a wind turbine blade using fbg sensors embedded in the blade bonding line," *Smart Materials and Structures*, vol. 22, no. 12, p. 125004, 2013.

[8] S. W. Doebling, C. R. Farrar, M. B. Prime, *et al.*, "A summary review of vibration-based damage identification methods," *Shock and vibration digest*, vol. 30, no. 2, pp. 91–105, 1998.

[9] C. Enei, G. Bernardini, J. Serafini, L. Mattioni, C. Ficuciello, and V. Vezzari, "Photogrammetric detection technique for rotor blades structural characterization," in *Journal of Physics: Conference Series*, vol. 658, p. 012003, IOP Publishing, 2015.

[10] G. Bernardini, J. Serafini, C. Enei, L. Mattioni, C. Ficuciello, and V. Vezzari, "Structural characterization of rotor blades through photogrammetry," *Measurement Science and Technology*, vol. 27, no. 6, p. 065401, 2016.

[11] L. Trainelli, M. Gennaretti, E. Zappa, M. Lovera, A. Rolando, P. Cordisco, R. Grassetti, and M. Redaelli, "Development and testing of innovative solutions for helicopter in-flight noise monitoring and enhanced control based on rotor state measurements," in *Proceedings of 42nd European Rotorcraft Forum, Lille, France*, September 2016.

[12] G. C. Kirby III, T. W. Lim, R. Weber, A. Bosse, C. Povich, and S. Fisher, "Strain-based shape estimation algorithms for a cantilever beam," in *Smart Structures and Materials' 97*, pp. 788–798, International Society for Optics and Photonics, 1997.

[13] R. Glaser, V. Caccese, and M. Shahinpoor, "Shape monitoring of a beam structure from measured strain or curvature," *Experimental mechanics*, vol. 52, no. 6, pp. 591–606, 2012.

[14] G. Foss and E. Haugse, "Using modal test results to develop strain to displacement transformations," in *Proceedings of the 13th international modal analysis conference*, vol. 2460, p. 112, 1995.

[15] P. B. Bogert, E. Haugse, and R. E. Gehrki, "Structural shape identification from experimental strains using a modal transformation technique," in *Proceedings of 44th AIAA/ASME/ASCE/AHS Structures, Structural Dynamics and Materials Conference, Norfolk, Virginia*, 2003.

[16] C.-g. Pak, "Wing shape sensing from measured strain," *AIAA Journal*, vol. 54, no. 3, pp. 1068–1077, 2016.

[17] M. Alioli, P. Masarati, M. Morandini, T. Carpenter, N. B. Osterberg, and R. Albertani, "Membrane shape and load reconstruction from measurements using inverse finite element analysis," *AIAA Journal*, vol. 55, no. 1, pp. 297–308, 2017. doi:10.2514/1.J055123.

[18] D. H. Hodges and E. H. Dowell, "Nonlinear equation for the elastic bending and torsion of twisted nonuniform rotor blades," Tech. Rep. TN D-7818, NASA, 1974.

[19] S. W. Doebling, C. R. Farrar, M. B. Prime, and D. W. Shevitz, "Damage identification and health monitoring of structural and mechanical systems from changes in their vibration characteristics: a literature review," tech. rep., Los Alamos National Lab., NM (United States), 1996.

[20] H. Sohn, C. R. Farrar, F. M. Hemez, D. D. Shunk, D. W. Stinemates, B. R. Nadler, and J. J. Czarnecki, "A review of structural health monitoring literature: 1996–2001," *Los Alamos National Laboratory, USA*, 2003.

[21] R. B. Randall, “State of the art in monitoring rotating machinery-part 1,” *Sound and vibration*, vol. 38, no. 3, pp. 14–21, 2004.

[22] R. B. Randall, “State of the art in monitoring rotating machinery-part 2,” *Sound and Vibration*, vol. 38, no. 5, pp. 10–17, 2004.

[23] D. Montalvao, N. M. M. Maia, and A. M. R. Ribeiro, “A review of vibration-based structural health monitoring with special emphasis on composite materials,” *Shock and Vibration Digest*, vol. 38, no. 4, pp. 295–326, 2006.

[24] P. Welch, “The use of fast fourier transform for the estimation of power spectra: a method based on time averaging over short, modified periodograms,” *IEEE Transactions on audio and electroacoustics*, vol. 15, no. 2, pp. 70–73, 1967.

[25] P. Masarati, M. Morandini, and P. Mantegazza, “An efficient formulation for general-purpose multibody/multiphysics analysis,” *Journal of Computational and Nonlinear Dynamics*, vol. 9, no. 4, p. 041001, 2014. doi:10.1115/1.4025628.

[26] C.-J. Li and A. G. Ulsoy, “High-precision measurement of tool-tip displacement using strain gauges in precision flexible line boring,” *Mechanical Systems and Signal Processing*, vol. 13, no. 4, pp. 531–546, 1999.

[27] D. P. Raymer, *Aircraft Design: A Conceptual Approach and Rds-student, Software for Aircraft Design, Sizing, and Performance Set (AIAA Education)*. AIAA (American Institute of Aeronautics & Ast, 2006.